AGU PUBLICATIONS

Geophysical Research Letters

RESEARCH LETTER
10.1002/2016GL069035

Special Section:
First results from NASA's Magnetospheric Multiscale (MMS) Mission

Wave telescope technique for MMS magnetometer

Y. Narita[1], F. Plaschke[1], R. Nakamura[1], W. Baumjohann[1], W. Magnes[1], D. Fischer[1], Z. Vörös[1], R. B. Torbert[2], C. T. Russell[3], R. J. Strangeway[3], H. K. Leinweber[3], K. R. Bromund[4], B. J. Anderson[5], G. Le[4], M. Chutter[2], J. A. Slavin[6], E. L. Kepko[4], J. L. Burch[7], U. Motschmann[8,9], I. Richter[10], and K.-H. Glassmeier[10,11]

[1]Space Research Institute, Austrian Academy of Sciences, Graz, Austria, [2]Institute for the Study of Earth, Oceans, and Space, University of New Hampshire, Durham, New Hampshire, USA, [3]Institute of Geophysics and Planetary Physics, University of California, Los Angeles, California, USA, [4]NASA Goddard Space Flight Center, Greenbelt, Maryland, USA, [5]The Johns Hopkins University Applied Physics Laboratory, Laurel, Maryland, USA, [6]Department of Atmospheric, Oceanic and Space Sciences, University of Michigan, Ann Arbor, Michigan, USA, [7]Southwest Research Institute, San Antonio, Texas, USA, [8]Institut für Theoretische Physik, Technische Universität Braunschweig, Braunschweig, Germany, [9]Institut für Planetenforschung, Deutsches Zentrum für Luft- und Raumfahrt, Berlin, Germany, [10]Institut für Geophysik und Extraterrestrische Physik, Technische Universität Braunschweig, Braunschweig, Germany, [11]Max-Planck-Institut für Sonnensystemforschung, Göttingen, Germany

Key Points:
- First-time determination of magnetosheath turbulence properties in the ion-kinetic range
- First-time successful application of interferometric method to MMS magnetometer data
- Discovery of dispersive character of mirror mode in the ion-kinetic range

Correspondence to:
Y. Narita,
yasuhito.narita@oeaw.ac.at

Citation:
Narita, Y., et al. (2016), Wave telescope technique for MMS magnetometer, *Geophys. Res. Lett.*, *43*, 4774–4780, doi:10.1002/2016GL069035.

Received 6 APR 2016
Accepted 5 MAY 2016
Accepted article online 11 MAY 2016
Published online 24 MAY 2016

Abstract Multipoint measurements are a powerful method in studying wavefields in space plasmas. The wave telescope technique is tested against magnetic field fluctuations in the terrestrial magnetosheath measured by the four Magnetospheric Multiscale (MMS) spacecraft on a spatial scale of about 20 km. The dispersion relation diagram and the wave vector distribution are determined for the first time in the ion-kinetic range. Moreover, the dispersion relation diagram is determined in a proxy plasma rest frame by regarding the low-frequency dispersion relation as a Doppler relation and compensating for the apparent phase velocity. Fluctuations are highly compressible, and the wave vectors have an angle of about 60° from the mean magnetic field. We interpret that the measured fluctuations represent a kinetic-drift mirror mode in the magnetosheath which is dispersive and in a turbulent state accompanied by a sideband formation.

1. Introduction

Adaptive filter techniques for multipoint measurements offer a variety of analysis methods for in situ spacecraft observations in space plasma physics. The wave telescope technique developed in the 1990s and early 2000s [*Neubauer and Glassmeier*, 1990; *Pinçon and Lefeuvre*, 1991; *Motschmann et al.*, 1995, 1996; *Glassmeier et al.*, 2001] is most successfully applied to studying waves and turbulence properties using four-point magnetometer data from the Cluster mission [*Escoubet et al.*, 2001]. The wave telescope technique is a minimum variance analysis and is a branch of maximum likelihood methods for a Gaussian likelihood function. The essence of the technique is that one can determine the fluctuation amplitude as a function of not only frequencies but also three components of wave vectors within the limit of a spatial sampling distance. Applications using the wave telescope include an observational estimate of wave vectors, dispersion relations, wave propagation speeds and directions, magnetic helicity density, bispectrum in the wave vector domain, and turbulence energy spectrum. A monograph by *Narita* [2012] summarizes these wave telescope applications in detail. Furthermore, using the wave vectors in three dimensions, the wave telescope technique enables one to estimate the frequencies in the plasma rest frame by correcting for the Doppler shift.

With the advent of the Magnetospheric Multiscale (MMS) mission [*Burch et al.*, 2016] it becomes possible to extend the wave telescope technique from the Cluster tetrahedral scale (ranging from 10,000 km down to 100 km) to the kinetic scales of space plasma phenomena at about 10 km. After the launch on 13 March 2015 and subsequent flight maneuvers, the MMS spacecraft were set to an equatorial orbit to measure the diffusion region of magnetic reconnection at the dayside magnetopause. MMS spacecraft formed a nearly regular tetrahedron and measured the dayside magnetosheath plasma at a distance of about 10 R_E, which is ideal to test the wave telescope technique against the MMS magnetometer data in the Earth magnetosheath region.

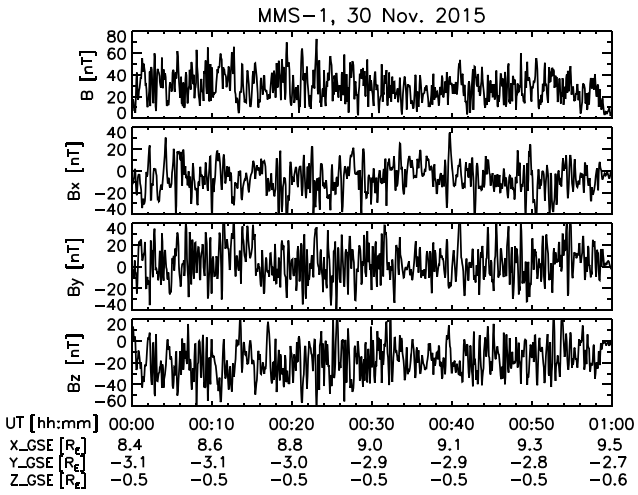

Figure 1. Time series plot of (first panel) MMS-1 magnetic field magnitude and (second to fourth panels) three components on 30 November 2015.

We present a wavefield study in the magnetosheath at wavelengths down to about 20 km as an application of the wave telescope technique to the MMS magnetometer data. This length scale corresponds to a kinetic range between the ion inertial length (about 300 km in this study) and the electron inertial length (about 7 km). We use the magnetic field data from the fluxgate magnetometer (FGM) on board MMS, L2 (level 2) survey mode at a sampling rate of 16 Hz (downsampled data) [*Russell et al.*, 2014; *Torbert et al.*, 2014]. We use an extended version of the wave telescope technique, Multi-point Signal Resonator (MSR) algorithm developed by *Narita et al.* [2011]. The MSR algorithm incorporates an eigenvalue-based analysis method, Multiple Signal Classification or MUSIC [*Schmidt*, 1986], with a generalization to the problem to the unknown numbers of signals [*Choi et al.*, 1993], into the wave telescope technique and achieves an improved signal-to-noise ratio in the wave vector analysis.

2. Data Analysis

2.1. Magnetosheath Event

MMS observation on 30 November 2015, 0010–0050 UT, is selected for the test of the wave telescope in the magnetosheath since the magnetic field fluctuations are quasi-stationary. MMS is located in the dayside magnetosheath with interspacecraft distances ranging from 22.9 km (between spacecraft 1 and 2) to 13.0 km (spacecraft 3 and 4). Reciprocal vector lengths of the spacecraft coordinates are from 0.58 rad/km (normal to the plane spanning spacecraft 1, 2, and 3) to 0.34 rad/km (spacecraft 2, 3, and 4). The fractal dimension as measured by the Q_G index [*von Stein et al.*, 1992; *Robert et al.*, 2001] is $Q_G = 1 + \frac{S_{obs}}{S_0} + \frac{V_{obs}}{V_0} = 2.32$, where S_{obs} and V_{obs} denote the total surface area and the volume formed by four spacecraft and $S_0 = \sqrt{3}\ell^2$ and $V_0 = \sqrt{2}\ell^3/12$ for a regular tetrahedron using the maximum spacecraft separation distance ℓ. The spacecraft configuration during the measurement time represents a moderately distorted tetrahedron. We limit our analysis to a maximum wave number of 0.17 rad/km, which is the spatial Nyquist wave number. Magnetometer data from MMS-1 spacecraft are shown as a time series plot in Figure 1 in the GSE coordinate system. Magnetic field fluctuations appear both in compressible and shear components and attain higher amplitudes of about 10–20 nT.

2.2. Spectral Estimate

The time series data are transformed into the spectral data in the spacecraft-frame frequency domain using the fast Fourier transform (FFT) and the Welch algorithms. That is, the 40 min interval (0010–0050 UT) is divided into a set of 64 s subintervals (1024 data points for FFT); the data are transformed using fast Fourier transform; the procedure is repeated by shifting the time window by a size of 11.9 s (190 data points for the shift) and an overlap of *52.1* s.

The spectral data in the frequency domain are used to estimate 3×3 cross-spectral density matrices on a single spacecraft basis as a function of the frequencies. The matrix is averaged over the time subwindows and the four spacecraft to enhance the statistical significance. The wave power is obtained for the perpendicular and parallel fluctuating field components with respect to the mean magnetic field as a function of the spacecraft-frame frequencies and shown as power spectra in Figure 2 (top).

The power spectra exhibit the following features. First, the compressible component of fluctuation (parallel fluctuation power) has nearly the same order of magnitude as the perpendicular (or shear) fluctuation power. This feature persists in the entire analyzed frequency range from 0.01 to 8 Hz. The presence of a high fluctuation power in the compressible component is suggestive of the mirror mode, which is typical for the

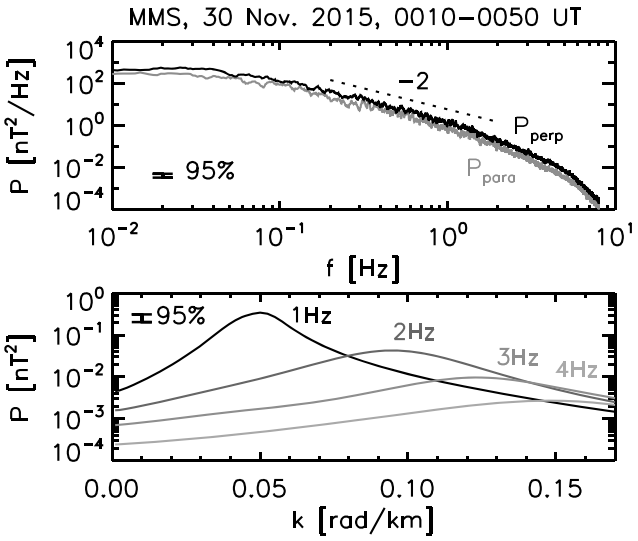

Figure 2. (top) Magnetic energy spectrum in the spacecraft-frame frequency domain averaged over four MMS spacecraft and (bottom) slices of the spectrum in the wave number domain at 1 Hz, 2 Hz, 3 Hz, and 4 Hz.

magnetosheath region. Second, the spectra show a smooth decay toward higher frequencies and do not show a clear peak. Because the fluctuation amplitudes are far above the instrumental noise level, the smooth spectra are suggestive of a turbulence-like energy spectrum. In fact, the spectral curve in the intermediate frequency range (from 0.1 Hz to 1 Hz) can reasonably represent a power law with a spectral index of −2. The spectral curve is flatter at lower frequencies below 0.1 Hz and steeper at higher frequencies above 1 Hz. Also, there is an indication of the spectral break at around 6 Hz.

The first spectral break at spacecraft-frame frequencies of about 0.1 Hz roughly agrees with the wave number for the maximum growth of the mirror mode swept by the flow. Using a proxy flow speed of 140 km/s (estimated later), the streamwise wave number for the breakpoint frequency is about 0.004 rad/km, while a typical wave number for the maximum growth rate of the mirror mode is about $0.4\Omega_p/V_A$ [*Gary*, 1993], which is estimated to be about 0.008 rad/km under a typical magnetosheath condition. Here Ω_p and V_A denote the proton gyrofrequency and the Alfvén speed, respectively. The formation of a power law spectrum with nearly random phases of fluctuations is indicative of a turbulent process, yet we do not know what kind of nonlinear processes are operating at the present stage. Candidate processes for the energy transport or cascade include eddy turnover (which is of hydrodynamic origin), wave-wave interactions involving linear mode or nonlinear mode types (which is of magnetohydrodynamic or kinetic plasma origin), or wave-particle-wave interactions (which is of purely kinetic nature). The second spectral break at frequencies of about 6 Hz can be interpreted either as a dissipation turbulent fluctuations or an excitation of high-frequency dispersive waves such as whistlers. In the former scenario, the fluctuation energy for the magnetic field is converted into the thermal energy. It is not clear which species contribute to the dissipation, protons or electrons, as the estimated spatial scale is about 13 times smaller than the proton inertial length yet only 3 times larger than the electron inertial length. In the latter scenario, the fluctuation energy is shifted more to the electric field (yet in the electromagnetic sense) due to the induction law.

The spectral data are further used to construct 12×12 generalized cross-spectral matrices using the four spacecraft as a function of the frequencies. Here 12 elements of the matrix represent three components of the magnetic field measured at four different spacecraft positions. The matrix is reduced into a 3×3 matrix (consisting of three components of the magnetic field) by the MSR interferometric projection onto the three-dimensional wave vector domain. The wave power is obtained by computing a trace of the 3×3 matrix. The wave power is scanned in the wave vector domain by spanning a spherical mesh with resolutions of 0.0025 rad/km in the wave vector magnitude and 1° in both polar and azimuthal angles. The scan is applied to each spacecraft-frame frequency up to 8 Hz.

Examples of the wave power in the wave number domain are shown in Figure 2 (bottom) at frequencies of 1 Hz, 2 Hz, 3 Hz, and 4 Hz.

The wave power represents an envelope of the maximum power over the polar and the azimuthal angles at each wave number, called the shell maximum power [*Glassmeier et al.*, 2001]. From low frequencies to higher ones, we observe (1) the wave numbers for the spectral peak increases, (2) the values of the spectral peak decrease, and (3) the spectrum becomes flatter. The shift of the peak wave numbers at higher frequencies indicates a dispersion relation.

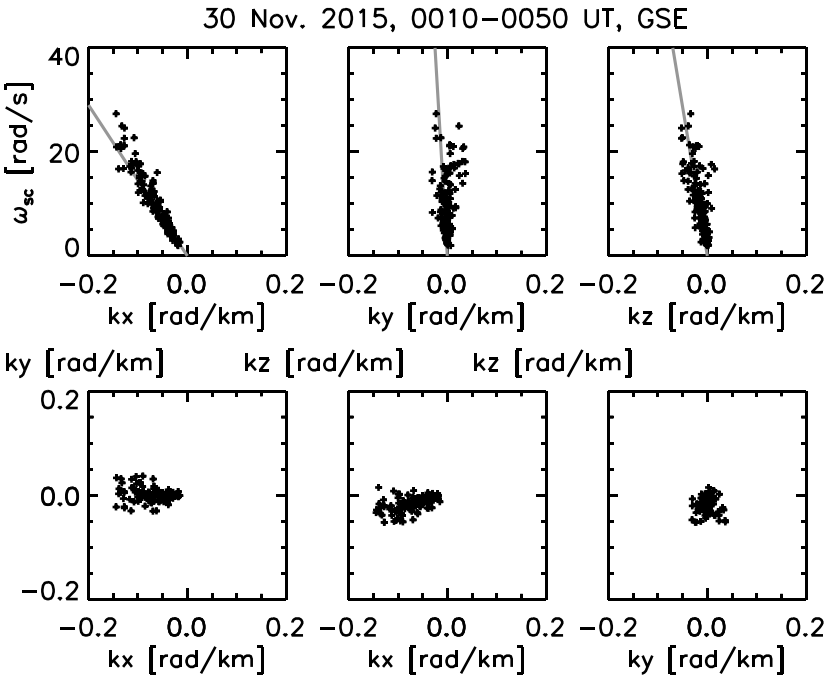

Figure 3. Distribution of the frequencies (in the spacecraft frame) and the wave vectors projected to the (top row) dispersion relation diagram and the (bottom row) wave vector diagram.

2.3. Dispersion Relation Diagram

The frequencies and the wave vectors for the spectral peaks are displayed as a scatterplot in six different projections: dispersion relation diagram (wave number-frequency domain) in three different directions of the GSE coordinate system (Figure 3, top row) and wave vector diagram (Figure 3, bottom row).

In Figure 3 (top row), the wave number-frequency diagram displays a clear dispersion branch, particularly at lower frequencies. The dispersion branch appears almost linear below 10 rad/s (or below 1.6 Hz), indicated by straight lines in gray in Figure 3. At higher frequencies the frequencies start to deviate from the low-frequency branch. The slopes of the linear dispersion branch represent the apparent phase velocities in the three directions and are obtained as $\omega_{sc}/k_x = -145$ km/s, $\omega_{sc}/k_y = -1600$ km/s, and $\omega_{sc}/k_z = -571$ km/s. The true phase velocity (in the spacecraft frame) is obtained from the apparent phase velocities using the conversion rule as $v_{ph} = \left[|\omega_{sc}/k_x|^{-2} + |\omega_{sc}/k_y|^{-2} + |\omega_{sc}/k_z|^{-2}\right]^{-1/2} = 140$ km/s. By projecting onto three directions using the unit vector $[k_x/\omega_{sc}, k_y/\omega_{sc}, k_x/\omega_{sc}]/\sqrt{|k_x/\omega_{sc}|^2 + |k_y/\omega_{sc}|^2 + |k_x/\omega_{sc}|^2}$, we obtain the three components of the true phase velocity as $v_{phx} = -135$ km/s, $v_{phy} = -12$ km/s, and $v_{phz} = -34$ km/s.

In Figure 3 (bottom row), wave vector directions are markedly antisunward ($-X$ component in GSE) with a moderate southward component ($-Z$ component). Scattering of wave vectors is less than 15° from the primary extension direction of the wave vectors. This fact confirms the estimated true phase velocities above.

Although the flow velocity information is not yet available at the current stage of the data analysis, one may derive the dispersion relation diagram in an approximative sense as follows. Because the highly compressible sense of fluctuations and the linear shape of the dispersion branch in the spacecraft frame are suggestive of the mirror mode, we use the low-frequency phase velocity estimated above as a proxy for the flow velocity. Using that velocity, the frequencies can be transformed into a compensated frame (or a proxy rest frame comoving with the plasma) using the Doppler relation as $\omega_{comp} = \omega_{sc} - \vec{k} \cdot \vec{V}_{ph}$. The dispersion relation diagram in the compensated frame, and the propagation angles as a function of the wave number are displayed in Figure 4. Wave number and angle errors are estimated from a half-value width of the spectrum. Phase velocity error is estimated from the scattering of wave vectors at an angle of about 15°, which imposes an error of about 4% in the phase velocity. Frequency error in the compensated frame is estimated through $\Delta(kv_{ph}) = \Delta k\, v_{ph} + k\Delta v_{ph}$.

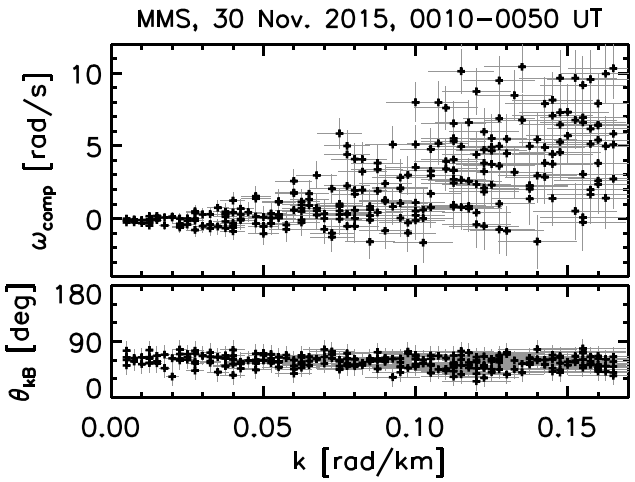

Figure 4. (top) Dispersion relation diagram with the frequencies compensated for the phase velocity of the low-frequency branch as a proxy of Doppler shift correction and (bottom) distribution of the wave vector angles from the mean magnetic field. Errors in the wave numbers represent the half-value width of the spectrum, and that in the frequencies represent the uncertainty in the Doppler shift correction.

The dispersion relation may be regarded as the zero frequency or of a linear type at lower wave numbers up to around 0.02 rad/km. Above that wave number, the dispersion relation diagram exhibits an increasing sense of both the frequency spread and the center of the frequency distribution (when sliced at a fixed wave number) at higher wave numbers. Only a small portion of the detected waves have a negative frequency in the proxy rest frame; i.e., most of the waves propagate away from the Sun in the proxy rest frame. The wave vector angles do not substantially change from lower to higher wave numbers. The mean propagation angle is 57.2 ± 9.6° from the mean magnetic field and is roughly along the antisunward direction with a deviation into the slightly southward direction. The wave vectors make a mean angle of 19.0 ± 10.3° from the antisunward direction (−*X* direction in the GSE coordinate system), 91.2 ± 10.8° from the duskward direction (+*Y* direction), and 105.2 ± 10.3° from the ecliptic north direction (+*Z* direction). The increasing sense of the frequency spread is suggestive of waves evolving from a linear mode into off-branch, sideband wave components. The increasing sense of the center of the frequency distribution indicates that the waves become dispersive such as that of the whistler mode in the kinetic domain.

In principle, it is possible to perform the polarization analysis in the plasma rest frame but that the estimator or definition of polarization must be carefully treated in the multispacecraft wave analysis. The notion of polarization (in the plasma physics convention) means a temporary field rotation sense when viewing into the direction of the mean magnetic field at a fixed spatial point and a positive frequency, while the helicity is a spatial field rotation sense around the wave vector at a fixed time [*Gary*, 1993]. Polarization is subject to the choice of the reference frame, while the helicity is an invariant to the Galilei transformation. From the wave telescope analysis one obtains a generalized polarization by combining the off-diagonal elements of the cross-spectral density matrix at a given set of frequency and wave vector. So far, it is known that the helicity density can be determined from the wave telescope technique [*Narita et al.*, 2009] but is not trivial how to obtain a proper estimate of the polarization by projecting the cross-spectral density matrix onto the rest frame frequency domain. The problem lies in the fact that the frequencies are irregularly distributed after the Doppler shift correction, and a suitable interpolation scheme must be developed for the polarization estimator in the rest frame.

The mean magnetic field magnitude is $B_0 = 37.1$ nT, proton gyrofrequency is $\Omega_p = 3.6$ rad/s, and that of an electron is $\Omega_e = 6526$ rad/s. We refer to the ion measurements from 190 magnetosheath intervals in the Cluster spacecraft data from February to June 2002 [*Narita et al.*, 2006] (because the final plasma data were not available at the time of preparation of the current work) and use a mean number density of ions $n_i = 23.4$ cm^{-3}. The Alfvén speed is then estimated as $V_A = 167$ km/s. The wave number for the proton inertial length is $\Omega_p/V_A = 0.021$ rad/km and that of an electron is $\sqrt{1836}\Omega_p/V_A = 0.91$ rad/km. Therefore, the dispersion relation we obtain here represents most likely waves in the ion-kinetic range. The phase speed in the proxy rest frame is of up to about 50 km/s, which is below the Alfvén speed. We interpret the measured magnetic field fluctuations as an ion-kinetic extension of the mirror mode with oblique propagation angles (θ_{kB} about 60°), wave dispersion (in an increasing sense of frequencies at higher wave numbers), and sideband wave components.

3. Discussion and Outlook

When the wave telescope technique was first applied to Cluster magnetometer data, it became apparent that Cluster is more than just a four-spacecraft mission, e.g., by *Glassmeier et al.* [2001]. This experience certainly applies to MMS as well. Multispacecraft observations, when combined with an adaptive filter technique, serves as a powerful tool in studying waves and turbulence in space plasmas. While the Cluster mission provides a spatial resolution of 100 to 200 km, our study shows that MMS can indeed allow us to extend a resolution of about 10 to 20 km. The wave telescope study shows that the wave numbers can be resolved at nearly 10 times higher than the ion inertial wave number in the magnetosheath. Of course, depending on the mean values of the magnetic field magnitude and the plasma density, there will be opportunities of a direct measurement in the electron-kinetic range.

The first-time wave telescope application to the MMS magnetometer data reveals that the magnetosheath fluctuations in the ion-kinetic range are characterized by the wave dispersion (i.e., deviation from the linear dispersion relation) and the formation of sideband wave components. Candidate wave modes for the detected waves include the whistler mode [*Smith and Tsurutani*, 1976; *Zhang et al.*, 1998; *Baumjohann et al.*, 1999], the ion cyclotron mode [*Czaykowska et al.*, 2001], and the kinetic modulation of the mirror mode [*Pokhotelov et al.*, 2001]. The scenarios for the low-frequency whistler waves or the ion cyclotron waves are unlikely because the estimated frequencies in the plasma rest frame are too low for the whistler waves but yet too high for the ion cyclotron waves at a propagation angle of about 60°. Moreover, the fluctuating field is highly compressible, which disagrees with the character of the whistler and the ion cyclotron waves. The drift mirror mode is a likely candidate such that the frequency is a function of the perpendicular component of the wave vector. The interpretation of the drift mirror mode implies that the plasma is nonuniform at spatial scales of ion kinetics and that the ion velocity distribution function has a positive gradient in the velocity space.

The mirror mode likely exists not only on the fluid scales but also in the ion-kinetic range with a dispersive effect in the sense that the frequencies become increasingly higher. Furthermore, the frequencies become more scattered, forming the sideband wave components. Studying physical properties of the kinetic-scale or kinetic-drift mirror mode offers an interesting topic for understanding the evolution of space plasmas into a turbulent state. The mirror mode is, naively speaking, regarded as a zero-frequency mode and is essentially a spatial structure without any intrinsic propagation speed. Various possibilities would be possible for a plasma to develop into turbulence. First, linear mode waves (mirror mode, in our case) become dispersive at higher wave numbers (wave turbulence picture). Second, frequencies deviate from the normal mode branch, developing into nonnormal mode (weak turbulence picture). Third, nonlinearity in the flow such as eddies and eddy splitting lead to turbulence such that the mirror mode fluctuations are passively advected by the flow motion (strong turbulence picture).

In the analyzed time interval in the magnetosheath, the assumption of the planarity seems to be valid for the following reasons. First, the time series data show quasi-stationary (in the sense that the mean value and the variance do not evolve in time), which implies spatial quasi-homogeneous fluctuations when using the ergodic hypothesis. Second, the wave telescope analysis for the magnetosheath fluctuations on the ion scale using the Cluster spacecraft observations on the scale of ion inertial length (at about 100 km) shows the existence of nearly zero-frequency mode and the perpendicular wave vectors [*Narita and Glassmeier*, 2005]. However, of course, it might be possible that other fluctuation geometries can more conveniently describe the measured data. Examples of nonplanar fluctuations in the magnetosheath may include magnetohydrodynamic self-consistent mirror mode structures using the Bessel functions [*Constantinescu*, 2002], spherically propagating waves using spherical Bessel functions [*Constantinescu et al.*, 2006], or phase-shifted waves [*Plaschke et al.*, 2008].

Moreover, technically speaking, the wave telescope technique offers a calibration method for the plasma flow measurement using the mirror mode fluctuations on the fluid scales at spatial lengths larger than the ion inertial length. This statement, however, needs to be studied in more detail when the plasma data become available for a further test.

Acknowledgments
The dedication and expertise of the Magnetospheric Multiscale (MMS) development and operations teams are greatly appreciated. Work at JHU/APL, UCLA, UNH, and SwRI was supported by NASA contract NNG04EB99C. We acknowledge the use of L2 survey fluxgate magnetometer (FGM) data of the MMS spacecraft that are stored at the MMS Science Data Center https://lasp.colorado.edu/mms/sdc/ and are available upon request. The Austrian part of the development, operation, and calibration of the DFG was financially supported by rolling grant of the Austrian Academy of Sciences and the Austrian Space Applications Programme with the contract FFG/ASAP-844377. K.-H.G. is financially supported by the Deutsches Zentrum für Luft- und Raumfahrt and the German Bundesministerium für Wiurtschaft und Energie under contract 50OC1402.

References

Baumjohann, W., R. A. Treumann, E. Georgescu, G. Haerendel, K.-H. Fornaçon, and U. Auster (1999), Waveform and packet structure of lion roars, *Ann. Geophys.*, *17*, 1528–1534, doi:10.1007/s00585-999-1528-9.

Burch, J. L., T. E. Moore, R. B. Torbert, and B. L. Giles (2016), Magnetospheric multiscale overview and science objectives, *Space Sci. Rev.*, *199*, 5–21, doi:10.1007/s11214-015-0164-9.

Choi, J., I. Song, and H. M. Kim (1993), On estimating the direction of arrival when the number of signal sources is unknown, *Signal Process.*, *34*, 193–205, doi:10.1016/0165-1684(93)90162-4.
Constantinescu, O. D. (2002), Self-consistent model of mirror structures, *J. Atmos. Sol. Terr. Phys.*, *64*, 645–649, doi:10.1016/S1364-6826(02)00024-X.
Constantinescu, O. D., K.-H. Glassmeier, U. Motschmann, R. A. Treumann, K.-H. Fornaçon, and M. Fränz (2006), Plasma wave source location using Cluster as a spherical wave telescope, *J. Geophys. Res.*, *111*, A09221, doi:10.1029/2005JA011550.
Czaykowska, A., T. M. Bauer, R. A. Treumann, and W. Baumjohann (2001), Magnetic field fluctuations across the Earth's bow shock, *Ann. Geophys.*, *19*, 275–287, doi:10.5194/angeo-19-275-2001.
Escoubet, C. P., M. Fehringer, and M. Goldstein (2001), The Cluster mission, *Ann. Geophys.*, *19*, 1197–1200, doi:10.5194/angeo-19-1197-2001.
Gary, S. P. (1993), *Theory of Space Plasma Microinstabilities*, Cambridge Atmospheric and Space Science Series, Cambridge Univ. Press, Cambridge, U. K.
Glassmeier, K.-H., et al. (2001), Cluster as a wave telescope—First results from the fluxgate magnetometer, *Ann. Geophys.*, *19*, 1439–1447, doi:10.5194/angeo-19-1439-2001, (correction in 21, 1071, 2003).
Motschmann, U., T. I. Woodward, K.-H. Glassmeier, and D. J. Southwood (1995), Wave field analysis by magnetic measurements at satellite arrays: Generalized minimum variance analysis, *Ads. Space Res.*, *18*, 315–319, doi:10.1016/0273-1177(95)00964-7.
Motschmann, U., T. I. Woodward, K.-H. Glassmeier, D. J. Southwood, and J. L. Pinçon (1996), Wavelength and direction filtering by magnetic measurements at satellite arrays: Generalized minimum variance analysis, *J. Geophys. Res.*, *101*, 4961–4966, doi:10.1029/95JA03471.
Narita, Y., and K.-H. Glassmeier (2005), Dispersion analysis of low-frequency waves through the terrestrial bow shock, *J. Geophys. Res.*, *110*, A12215, doi:10.1029/2005JA011256.
Narita, Y., K.-H. Glassmeier, K.-H. Fornaçon, I. Richter, S. Schäfer, U. Motschmann, I. Dandouras, H. Rème, and E. Georgescu (2006), Low-frequency wave characteristics in the upstream and downstream regime of the terrestrial bow shock, *J. Geophys. Res.*, *111*, A01203, doi:10.1029/2005JA011231.
Narita, Y., K.-H. Glassmeier, and G. Kleindienst (2009), Evaluation of magnetic helicity density in the wave number domain using multi-point measurements in space, *Ann. Geophys.*, *27*, 3967–3976, doi:10.5194/angeo-27-3967-2009.
Narita, Y., K.-H. Glassmeier, and U. Motschmann (2011), High-resolution wave number spectrum using multi-point measurements in space—The Multi-point Signal Resonator (MSR) technique, *Ann. Geophys.*, *29*, 351–360, doi:10.5194/angeo-29-351-2011.
Narita, Y. (2012), *Plasma Turbulence in the Solar System, SpringerBriefs in Physics*, Springer, Heidelberg.
Neubauer, F. M., and K.-H. Glassmeier (1990), Use of an array of satellites as a wave telescope, *J. Geophys. Res.*, *95*(19), 115–122, doi:10.1029/JA095iA11p19115.
Pinçon, J. L., and F. Lefeuvre (1991), Local characterization of homogeneous turbulence in a space plasma from simultaneous measurements of field components at several points in space, *J. Geophys. Res.*, *96*, 1789–1802, doi:10.1029/90JA02183.
Plaschke, F., K.-H. Glassmeier, O. D. Constantinescu, I. R. Mann, D. K. Milling, U. Motschmann, and I. J. Rae (2008), Statistical analysis of ground based magnetic field measurements with the field line resonance detector, *Ann. Geophys.*, *26*, 3477–3489, doi:10.5194/angeo-26-3477-2008.
Pokhotelov, O. A., M. A. Balikhin, R. A. Treumann, and V. P. Pavlenko (2001), Drift mirror instability revisited: 1. Cold electron temperature limit, *J. Geophys. Res.*, *106*, 8455–8463, doi:10.1029/2000JA000069.
Robert, P., A. Roux, C. C. Harvey, M. W. Dunlop, P. W. Daly, and K.-H. Glassmeier (2001), Tetrahedron geometric factors, in *Analysis Methods for Multi-Spacecraft Data*, edited by G. Paschmann and P. W. Daly, pp. 323–348, ISSI Scientific Report SR-001, ESA Publ. Div., Bern, Switz.
Russell, C. T., et al. (2014), *199*, 189–256, doi:10.1007/s11214-014-0057-3.
Schmidt, R. O. (1986), Multiple emitter location and signal parameter estimation, *IEEE Trans. Ant., Prop.*, *34*, 276–280, doi:10.1109/TAP.1986.1143830.
Smith, E. J., and B. T. Tsurutani (1976), Magnetosheath lion roars, *J. Geophys. Res.*, *81*, 2261–2266, doi:10.1029/JA081i013p02261.
Torbert, R. B., et al. (2014), The FIELDS instrument suite on MMS: Scientific objectives, measurements and data products, *Space Sci. Rev.*, *199*, 105–135, doi:10.1007/s11214-014-0109-8.
von Stein, R., K.-H. Glassmeier, and M. Dunlop (1992), A configuration parameter for the Cluster satellites, *Tech. Rep. 2/1992*, Institut für Geophysik und Meteorologie der Technischen Universität Braunschweig.
Zhang, Y., H. Matsumoto, and H. Kojima (1998), Lion roars in the magnetosheath: The Geotail observations, *J. Geophys. Res.*, *103*, 4615–4626, doi:10.1029/97JA02519.